A Fabrication Free, 3D Printed, Multi-Material, Self-Sensing Soft Actuator

Travis Hainsworth[1*], Lawrence Smith[1*], Sebastian Alexander[1], Robert MacCurdy[1]

Abstract—**Soft robotics offers a range of attractive features relative to traditional rigid robots, including rapid customization, inherently safer human-robot interactions, and continuous passive dynamics that enable morphological computation. Here we present an actuator with an integrated print-in-place strain sensor which is produced entirely via multi-material additive manufacturing and requires no post processing or manual fabrication steps. One natural application of this technology is the end effector of robotic arms; incorporating deformable actuators into a gripping mechanism allows for the safe integration of robotic assistance in human-occupied settings. While numerous soft robot actuators have been implemented without feedback, force sensing and proprioception are valuable signals to leverage in extending the capabilities of these systems. Prior approaches to integrating sensors into soft robot components have relied on manual processes, or specialized fabrication tools. Our work shows a novel method for automatically manufacturing soft pneumatically-driven actuators with embedded sensors through readily available 3D printing tools with no human fabrication required. Automatically manufacturing these sensor-actuator systems enables more complex, capable, and integrate-able designs, because the labor of assembly is eliminated; actuator-sensor designs that would be tedious or impossible to manufacture become tractable with our approach.**

Index Terms—**Soft Sensors and Actuators, Additive Manufacturing, Grippers and Other End-Effectors, Hydraulic/Pneumatic Actuators, Soft Robot Materials and Design**

I. INTRODUCTION

SOFT end effectors (Figure 1) enjoy use in automated grasping operations due, in part, to the hallmarks of flexible robots: safer human-robot interactions, adaptability to a variety of use-scenarios, and easy customizability. Additionally, they can exhibit more degrees of freedom per control input compared to traditional rigid end effectors, enabling robust grasping of arbitrary shapes. Soft robotic systems are also appealing because they offer the potential to fabricate many-degree of freedom structures in one automated manufacturing operation, although this benefit has only recently begun to be explored. The materials used to fabricate soft
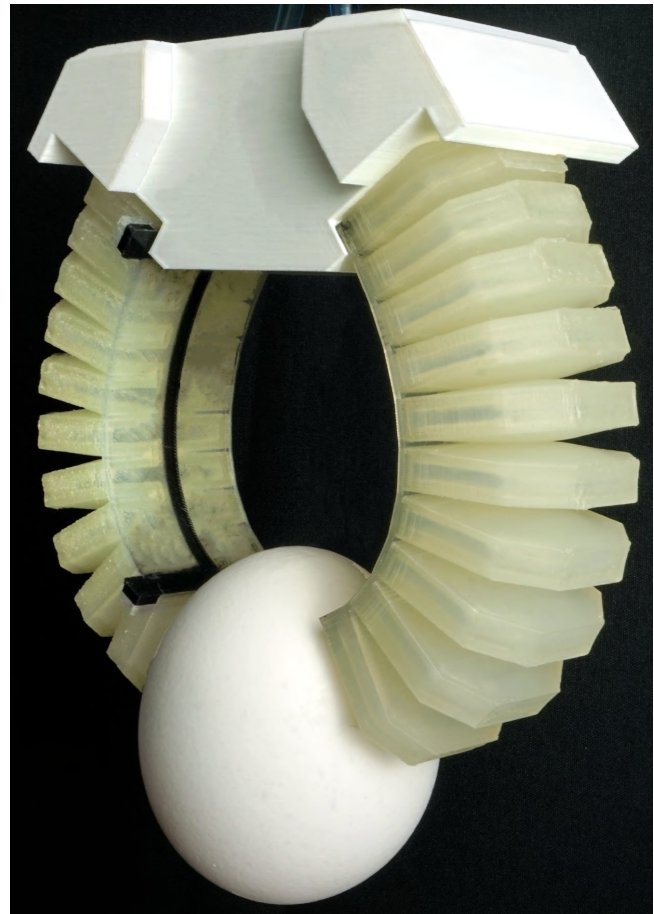
Fig. 1: An example gripper made with two of our print-in-place, self-sensing, soft actuators. These actuators are more compliant, yet can exert higher forces than related approaches (Figure 3) and incorporate a bend-angle sensor suitable for feedback control. In particular, the ability to exert higher forces, which expands the application envelope, can be enhanced by feedback position and force control in order to maintain the ability to interact with delicate objects. The entire sensor-actuator assembly is printed in a single step via multi-material 3D printing, requiring no manual fabrication steps.

actuators exhibit elongation-to-fracture properties which are orders of magnitude higher than conventional rigid robotic materials. This results in actuators that can respond elastically to unexpected large deformations without fracture, damaging other objects in the work space, or reduced function. Common practice in soft robotics is to construct compliant continuum actuators that have no proprioception; the natural dynamics of their soft materials allow them to conform to other objects in the environment, and their inherently modest force generation make these uncontrolled interactions less consequential than
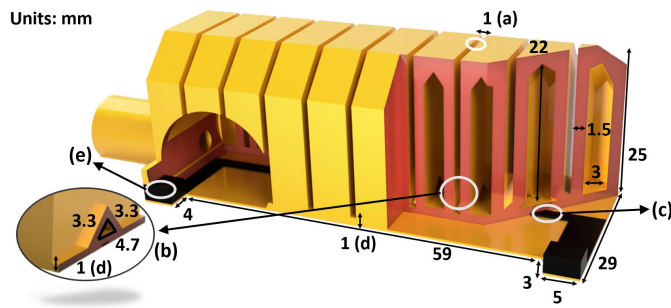
Fig. 2: This rendering of the 10 digit self-sensing actuator shows the small, buried features that are trivially manufactured through the use of AM. (a) By minimizing the space between adjacent digits, inflation is translated directly to a bending moment, with less energy stored in the elastic body. (b) Similarly, by minimizing the volume of the connecting channel between the digits less energy will be stored as stress in the medial plane (see Figure 4). (c) Minimizing the cross sectional area of the sensor's conductive material increases the resistance, easing measurements. (d) Minimized strain limiting layer aids large angular deflections. (e) Electrical connections to the sensor.
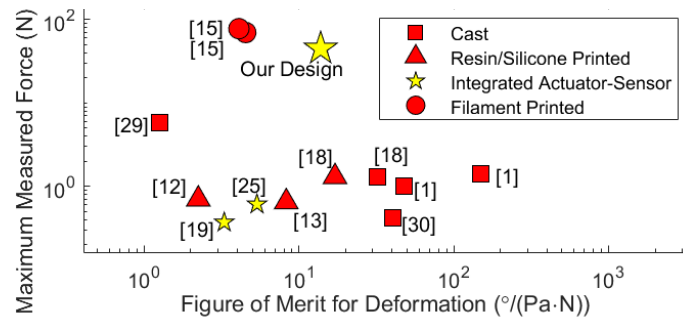

Fig. 3: Comparison plot, generated from data in related work, shows the conflicting design considerations of maximum force and actuator compliance; large numbers on each axis show proficiency in that metric. We define our deformation figure of merit as deflection in degrees divided by the product of length and applied pressure.

they would be with rigid robots. While many impressive results have been shown using this approach, compliant actuators capable of higher force might expand the application space, and control via integrated sensing would harness this higher force capability.

We present a soft, flexible, self-sensing actuator design (Figure 2) that exploits the unique geometric and material capabilities offered by Additive Manufacturing (AM) to create a print-in-place (fabrication requires no manual steps) sensor-actuator combination that is simultaneously very compliant and able to exert high force - a combination that places it on the frontier of the Pareto design space (Figure 3).

Our actuator design is related to the canonical PneuNet [1] approach, but differs in dimension and morphology. The PneuNet morphology was originally demonstrated with hyper-elastic materials that are shaped via casting; actuators fabricated in this way are characterized by high deformation at low actuation pressure and modest force-generation (Figure 3). Instead, we seek self-sensing actuators that can develop higher forces when pressurized, while reducing the strain energy lost when the inflation gas works on the material in the actuator itself (Figure 4), since such work is not done on the environment, and is lost during each cycle. This goal implies two opposing design objectives: stiffer materials can sustain higher pressures and generate more force, but they also require higher pressures to deform without any load, and store substantial actuation energy as internal stress.

Our contribution is a soft, self-sensing, highly-compliant actuator design that demonstrates a combination of compliance and force generation that balances these goals, which puts the design on the frontier of the Pareto design space compared to existing efforts. This is accomplished while incorporating a strain-sensor capable of providing feedback, and the print-in-place assembly requires no manual fabrication. We expect our work to be readily replicated because we leverage widely available multi-material additive manufacturing tools and materials to fabricate these actuators.

II. RELATED WORK

A sub-field of soft end effector research analyzes and improves soft actuators to enable rapid integration of efficient actuators into larger robotic assemblies [2]. The work on compliant actuators has explored methods like dielectric elastomers (DEAs) [3] which includes a robust self-healing variant [4]; these are manufactured by hand with a series of steps and provide high energy densities. Combustion has also been explored as a method of actuating soft robots [5][6]; this also provides high energy density. The most common soft actuators are various pneumatic networks [7] and exhibit many degrees of freedom in a single, continuous part. These have been modeled, analyzed extensively [8], and manufactured through a variety of methods, some of which we will enumerate here.

A. Casting

Pneumatic actuators have been primarily fabricated using mature processes such as casting [1], but these approaches access only a portion of the potential design space. This is due to the constraints associated with traditional manufacturing methods [9]. In addition to reducing the design space, manufacturing through casting is a tedious process that requires significant skill. Complex geometries often require multi-stage casts using techniques such as over molding.

B. Additive Manufacturing

AM is recognized for easing many of these fabrication constraints and enabling design geometries not reproducible by conventional methods. Additionally, multi-material AM provides a pathway to produce complex parts with widely varying mechanical properties while using little to no manual labor.

1) UV Curable: Previous work has explored methods for printing actuators with ultra-violet (UV) resins including Poly-Jet printing [18], and single material digital light projection (DLP) [19]. Zhang et al. fabricated a multi-material pneumatic actuator using PolyJet printing technology [10]. Peele et al. used Digital Mask Projection Stereolithography (DMPS) to fabricate small tentacle-like pneumatic actuators with multiple antagonistic pairs of actuator segments, capable of continuous motion in four directions [20]. Furthermore, portions of
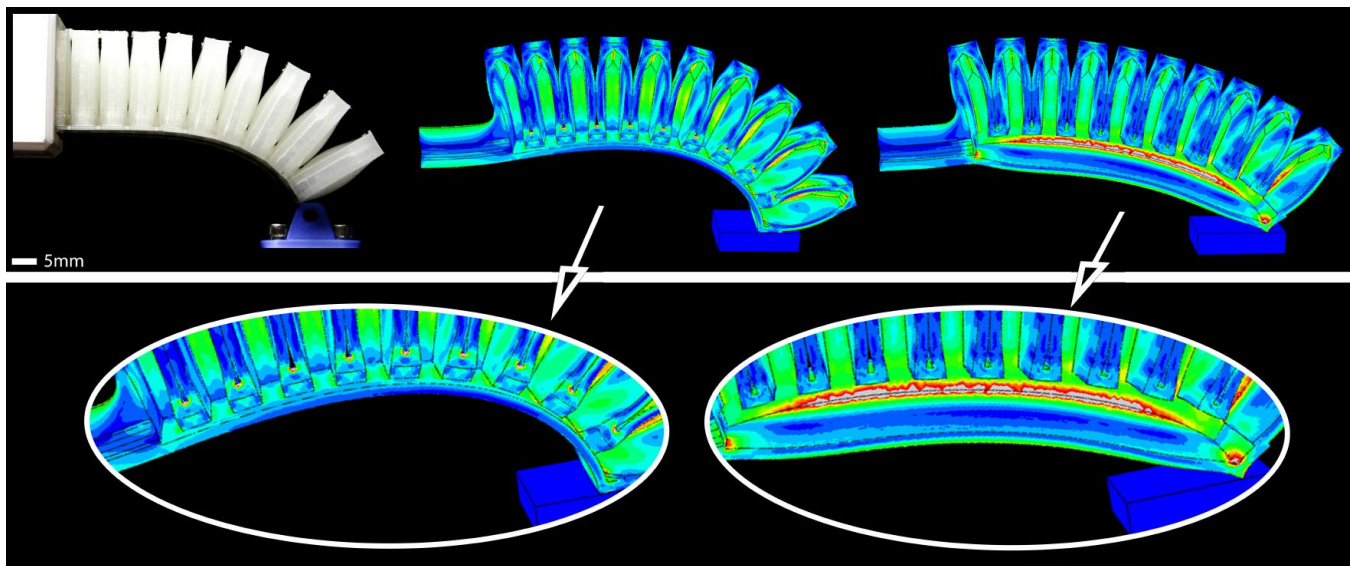
Fig. 4: Blocked-force testing of: (left) our 3D printed self-sensing actuator; (middle) an FEA stress analysis of our actuator using a hyperelastic constitutive model (Table I); (right) an FEA stress analysis of an actuator with channels and strain-limiting layers to match styles from previous work [8][10][11]-[17] using the same constitutive model. Our actuator design shows lower stress compared to designs derived from the canonical PneuNet (lower left vs lower right) because minimizing the cross-sectional area of the strain-limiting layer reduces the bending moment, and therefore less actuation energy is stored as elastic strain. This approach reduces the necessary working pressure for any given load.

HASEL actuators [4] have been additively manufactured with UV-curable resins that are then manually assembled into an actuator [21].

2) Fused Filament Fabrication: Fused Filament Fabrication (FFF), in which thermoplastic is extruded from one or more heated nozzles and builds an object layer-by-layer, is an appealing method for manufacturing due to its accessibility, low cost, and native support for a diverse set of materials. Additionally one of FFF's appeals is that the machines are easily customized: Yirimbesoglu et al. have demonstrated 3D printing of soft actuators using a Cartesian printer with a customized print head to mix and deposit a quick-setting two-part silicone rubber [14]. Byrne et al. have demonstrated the AM of soft tubular pneumatic actuators by careful injection of silicone rubber onto a rotating cylindrical substrate [13] which was used to create bio-inspired actuators [12]. Soft actuators fabricated with FFF have also been demonstrated using conventional printing hardware and materials. Yap. et al. developed and printed single and bi-directional pneumatic actuators using commercially available printing filament on an unmodified printer, as well as generating simulated and empirical test data to fully characterize their high-force design [11]. There are also AM cable-driven soft actuators which utilize cables and crimps manually inserted post-print [22].

C. Soft Strain Sensors

Integrating sensors into actuators is a less explored field. Mousavi et al. [23] have demonstrated a responsive electrical resistance-based strain and pressure sensor fabricated with AM, and a similar resistive sensor has been created using a poly-jet machine (UV curable resins) [24]. Previous work has manually injected liquid metal into AM actuators and used that to measure changes in resistance [25]. Tawk et al. [26] created

a self-sensing, soft actuator that requires tendon assembly post-print and uses commercial pressure sensors to estimate deflection. Actuators designed to be used in prosthetics [17] have been modified to incorporate pressure sensors, which are manually integrated into the finger/actuator after fabrication, to allow self-sensing capabilities. Truby et al. [15] created an actuator with an integrated sensor through a three step process: the base was cast, the sensor was printed into the base (a process known as multi-material, embedded 3D printing, EMB3D), and finally the top was cast to create the unified assembly. It has also been shown that a sensor can be printed in tandem with its actuator [16] with an Poly-jet machine; this process is only possible with encapsulated support material which has to be extracted manually, this labor intensive step constrains possible geometries and this actuator was designed as a two part system which was manually assembled.

While each of these prior methods demonstrate components of the overall vision of automatically fabricating a soft actuator with self-sensing capability that can be integrated seamlessly into a robotic assembly, none have yet achieved this goal. Our work advances the capability of multi-material, AM of soft actuators and shows a self-sensing, soft actuator created in a *single*, assembly free, automated manufacturing process.

III. CONTRIBUTIONS

Our contribution demonstrates a compliant actuator design that exhibits high force and low storage modulus simultaneously, a combination of compliance and force generation that lies on the Pareto front among existing efforts. We created a metric that allows diverse prior works to be scored for compliance and force generation, and used it to compare 13 prominent soft-robotics results. Our continuum actuator incorporates a self-sensing capability that enables the bending angle to be determined through a $50°$ range via a facile

resistive sensing element. We also show that this resistance sensor can be used to identify contact with other objects in the environment. Additionally, we show that a fabrication approach based on commodity tools and materials can be used to create multi-material soft robotic structures via a process that requires no manual assembly steps. Finally, we developed a set of configuration parameters for commercially available tools and materials that will allow others to easily replicate our results.

IV. METHODS

A. Actuator

In contrast to many previous 3D-printed soft actuators, we created a design that achieves large deflections at modest internal pressures (Figure 5) while maintaining the ability for high force output (Figure 3). This has two benefits: first, lower required working pressures enable smaller, lower-cost pressure sources; second, soft actuator designs that respond to lower pressures store less energy in their structures during actuation (Figure 4). Since there is no current method to recover this energy on each cycle, stiffer designs exhaust more energy per cycle - an undesirable quality for energy-constrained systems like mobile robots. To this end, we attempted to maximize deflection per unit pressurization while remaining within the printer's constraints and maintaining a reasonable print time. One significant departure from common soft actuator designs (Figure 4 right) we made was to reduce the area of the internal solid volume at the "spine" of the actuator (the strain-limiting region of the canonical soft actuator) by collapsing it to a small triangular region at the medial plane (Figure 2b shows dimensions). This lowers the bending stiffness of the actuator drastically, reducing the input energy required
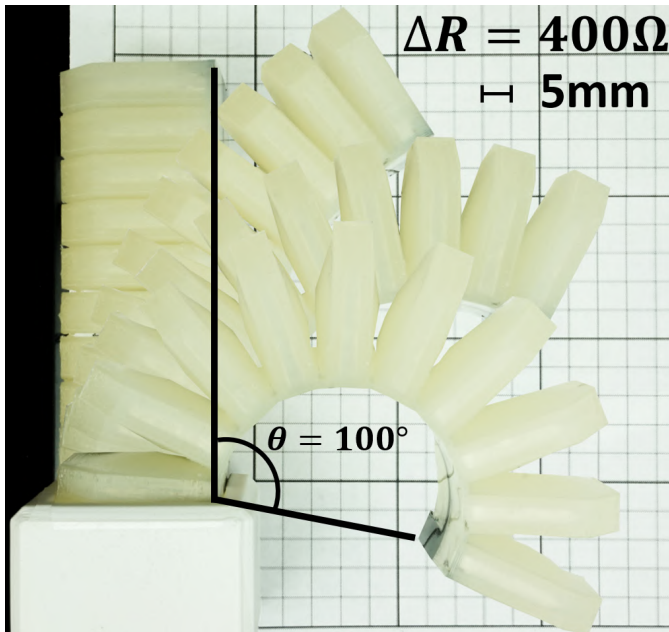

Fig. 5: When pressurized to 100 kPa these print-in-place, soft actuator-sensors have a bend angle of $\theta = 100°$ and measure a change in resistance of 400 Ω.

TABLE I: FEA Model Parameters

Mesh		Ogden Parameters			
Type	Quad Tet C3D10	μ_1	-30.921	α_1	0.508
Elements	107198	μ_2	10.342	α_2	1.375
		μ_3	26.791	α_3	-0.482

to achieve the desired mode of deflection (Figure 4). Such a design would be challenging to manufacture via casting [1], but is trivial to fabricate with FFF. We further reduced bending stiffness by minimizing the wall thickness between interior pressurized volumes and the exterior, while balancing the thickness required to prevent inter-layer leaks (Table II). Additionally, we minimized the inter-digit spacing on both the exterior and interior of the model (Figure 2a); this causes the walls of the digits to contact each other soon after pressure is applied, and this contact induces a bending moment (Figure 4).

B. Sensor

Soft 3D printable strain gauges can be manufactured using off-the-shelf, FFF 3D printers and commercially available conductive and flexible materials [23]. The sensitivity is governed by:

$$\frac{\Delta R}{R_0} = \frac{A_0 * L_f - A_f * L_0}{A_f * L_0} \qquad (1)$$

where R_0 is the starting resistance and ΔR is its change, A is the cross-sectional area, and L is the length of the conductive band; subscripts $_0$ and $_f$ refer to initial and final configurations, respectively, and we assume that volume in the resistor is conserved. Since relatively larger values of ΔR ease measurements, we prefer larger L_0 and smaller A_0, though these are limited by fabrication capabilities. We chose to print the sensor two layers thick in a crosshatch pattern; using two layers decreases the likelihood of separation between adjacent tracks of conductive filament (which would cause an open-circuit). Similar arguments informed the width and length of the sensing strip (Figure 2c).

C. Self-Sensing Actuator

Combining the 3D printed strain gauge and the 3D printed pneumatic actuator into one human-free manufacturing process results in a self-sensing, soft actuator which is delicate enough for soft grasps while simultaneously providing feedback. The integrated strain gauge is implemented on the medial surface (Figure 2c), and while it is true that there are locations farther from the neutral axis, and in turn, that this choice will reduce the sensitivity to bending, by choosing this plane we ensure that the gauge will be in compression when the actuator is pressurized. By ensuring that actuation compresses the gauge, the conductive filament will be pressed together and will aid electrical continuity. In contrast, when the gauge is in tension the filament may separate, which influences the resistance in an un-repeatable manner, and under large strains will fracture the filament; this fracturing would render the gauge unusable. The stereolithography (STL) files for this two-material design are available upon request.
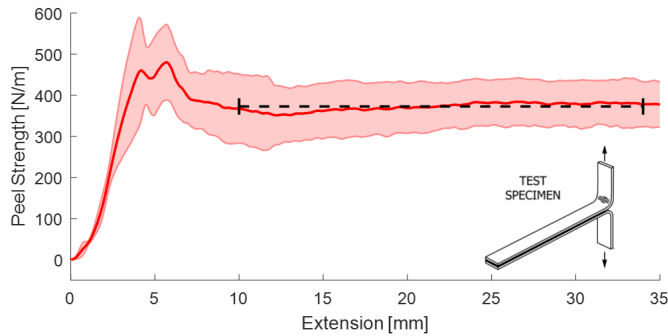
Fig. 6: Peel strength results of conductive PLA co-printed between TPU (NinjaFlex), tested according to ASTM D1876-08 on an Instron load frame. A peel strength of 370 N/m is calculated by averaging over the interval indicated in black in accordance with [27]. Shaded regions show 95% (2σ) confidence bounds of peel strength, n=6.

TABLE II: Slicer Settings

Universal				
Infill	18%			
Nozzle Diameter	0.35 mm		**Flexible TPU**	
Retract Speed	600 cm/min		Ext. Multiplier	2.12
Layer Height	0.15 mm		Ext. Width	0.2 mm
Top Layers	8		Retraction	1.5 mm
Bottom Layers	3		Restart Distance	-0.5 mm
Perimeters	4		Temperature	225°c
Bed Temp	70°c			
Cooling Fan	0%		**Conductive PLA**	
Print Speed	110 cm/min		Ext. Multiplier	1.01
Outline Speed	60%		Ext. Width	0.4 mm
			Retraction	2.00 mm
Ironing			Restart Distance	-0.03
Ext. Multiplier	1.5		Temperature	215°c
Ext. Width	0.3 mm			
Temperature	225°c			

D. Modeling

We compared the physical results to a finite element analysis (FEA) model (Figure 4) of the actuator design in a blocked force test. The simulation was executed using the commercial FEA code Abaqus™, with parameters for the Ogden hyper-elastic material model taken from [11], which performs mechanical characterization of the material our actuator is printed from (NinjaFlex, NinjaTek). In this simulation, the base of the actuator is fixed, and a uniform pressure load is applied to the interior cavity. Contact mechanics are enforced between the tip of the actuator and the block, as well as between the faces of adjacent digits. The block is fixed in space and additional simulation parameters are given in Table I. These simulations (Figure 4) demonstrate the efficacy of our design choices, relative to the common PneuNet derived designs. By minimizing the thickness of the strain limiting layer, which requires creating a discrete region for the air tube that connects bellows folds (Figure 2b,d), and by creating a larger number of smaller bellows folds, the internal stress is reduced. This reduces the energy stored when the actuator is deformed. Fabricating our alternative geometry via a casting approach might be possible, but it would be difficult because unlike most PneuNet derived designs, there is not a single cutting plane that cleanly separates the model and allows a planar pour to seal the model in a second step. However, this design is readily fabricated via FFF.

TABLE III: Notable Component Part Numbers of Apparatus

Pressure Controller	VEAB-L-26-D7-Q4-A4-1-R1
Flowrate Sensor	SFTE-10-U-Q4-B-Q3M8
Pressure Sensor	ProSense PTD25-20-0030H
Resistance Measurement	LabJack LJTR 10k
Data Acquisition	LabJack U6 Pro

E. Manufacturing

The combined sensor-actuator was entirely 3D printed in one process with a dual nozzle, two-material printer (MakerGear MK3ID). An initial layer of flexible material is deposited, then for the next two layers the sensor is printed in tandem with the actuator. This is accomplished by depositing molten conductive filament immediately after depositing the flexible material to create a physical bond between the two materials. This bond exhibits a 370 N/m peel strength (Figure 6). The actuator was printed with thermoplastic polyurethane (TPU) (NinjaFlex, NinjaTek) and the integrated sensors were printed with ProtoPasta's Carbon Black doped Polylactic acid (PLA). We used Simplify3D to slice the STL. The slicer settings are given in Table II and the .fff file is available upon request. To ensure an airtight seal at the top of the actuator, ironing was implemented on the last two layers of the print. Ironing is accomplished by having the hot nozzle automatically retrace a layer, at a 90° angle to the last layer while under-extruding material. The heat from the nozzle and the perpendicular print direction mesh each print line to form a more planar and airtight layer.

F. Test Apparatus

We designed and fabricated a test fixture (Figure 7, Table III) capable of applying a digitally controllable pneumatic pressure to our actuator, as well as measuring several output signals synchronously:

- variable resistance of the integrated strain sensor
- force developed at the tip of the soft actuator
- mass flowrate of air through the test fixture
- inlet pressure of the actuator

The fixture passes compressed air through a filter before delivering it to a proportional pressure controller capable of supplying the downstream system with a regulated pressure between 0 and 100 kPa. The air passes through a throttling valve to reduce oscillations and a flowrate sensor before reaching the connection point with the soft actuator under test. The pressure is measured here using a pressure transducer with a range of 0 to 200 KPa. Finally, a parallel-beam load cell on an adjustable x-y stage measures force developed at the tip of the actuator, and a precision voltage divider circuit measures the resistance of the integrated strain sensor.

The fixture is controlled with a MATLAB interface, which sends commands to and receives data from the data acquisition module as seen in Figure 7 lower. For the tests described in this paper, pressure set-points were delivered to the pressure controller at 10Hz, and signals were obtained from the fixture at 40 Hz. Figure 8 shows the actuator's mechanical and electrical responses to prescribed pressure as measured by the test fixture.
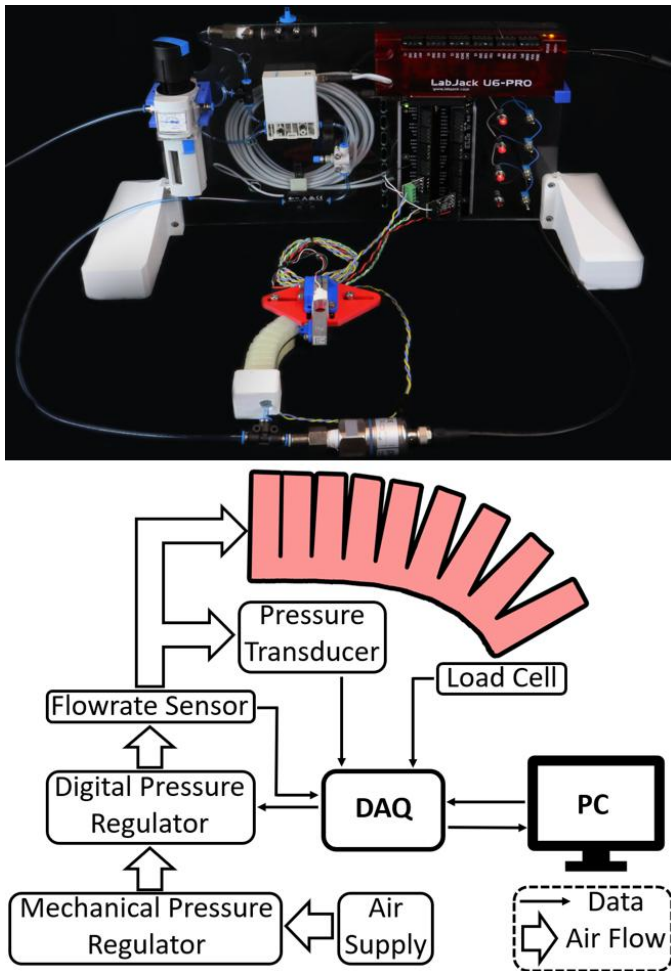
Fig. 7: Upper: With this custom test fixture we can measure the blocked force as we prescribe and measure pressure, as well as measuring the resistance from the strain gauge and the mass flowrate, which describes the air-tightness of the actuator. Lower: An input pressure is prescribed by a PC and then the data acquisition device (DAQ) measures actuator pressure, flowrate, force output, and integrated strain sensor readings at 40 Hz, up to 100 kPa.

G. Design Effectiveness

To compare the effectiveness of our actuator design we created the comparison plot shown in Figure 3 which compares an actuator's ability to deform with the maximum force that it can exert. We chose to characterize the compliance of a generic soft actuator by dividing the angular displacement of the actuator by the product of the length of the actuator and the pressure required to achieve the deformation. This forms our compliance figure of merit; higher compliance leads to more bending, even if the actuator is short and has lower driving pressures. Maximum exerted force is then compared; maximum force is chosen due to our interest in actuators capable of manipulating macro scale items. We collected this data set from related works, where available, to compare these two metrics. In this work, maximum force is measured with a manually controlled pressure input up to 441 kPa, following the procedure demonstrated by yap et al. [15], resulting in a maximum force of 45 N. All other measurements in this work are done with a maximum pressure of 100 kPa as this is the upper limit of controllability for our digital test apparatus.
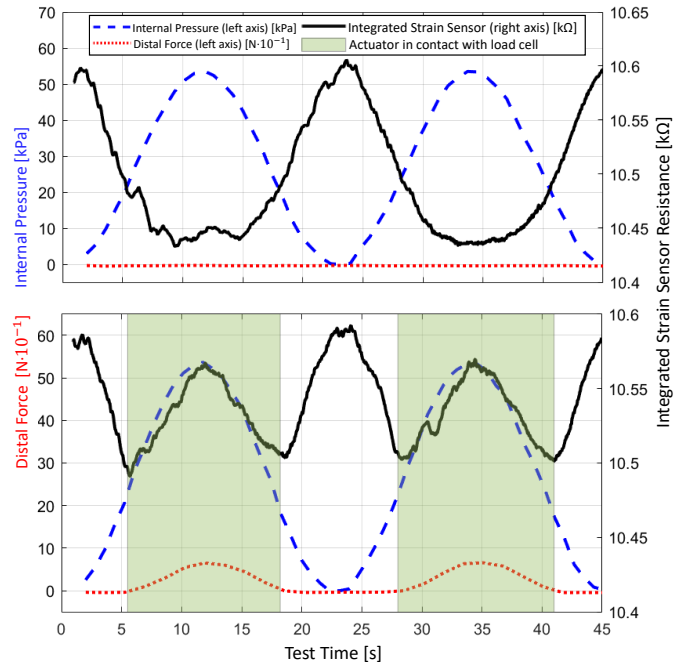

Fig. 8: Sensor response during free (upper) and grasping (lower) actuation with prescribed sinusoidal input pressure. Sensor resistance (solid) varies inversely with input pressure (dash) because the spine of the actuator is in compression, and the resistance changes dramatically when contact is made (shaded regions in lower) with the offset load cell (dots). Changes in resistance from baseline can be used to estimate tip bend angle as well as contact with external objects. Data were collected at 40 Hz.

The comparison plot shown in Figure 3 shows that our design is on the Pareto front of balancing maximum force against compliance.

V. RESULTS

The result of this work is a fully automated method for fabricating soft actuators with integrated feedback through an embedded print-in-place strain gauge which is capable of accurately estimating its position through 50° of deflection with a 95% confidence of fitting within ±10% error bounds (see Figure 10 inset) and requires no human interaction in fabrication. Each actuator is individually calibrated by manually bending it over mandrels of various diameters and measuring the change in electrical resistance for each constant angle. A 2nd-order best fit curve is fit to the data, with the form:

$$C(\Delta r) = a_0 (\Delta r)^2 + a_1 \Delta r + a_2 \quad (2)$$

where a_i are coefficients, Δr is the change in electrical resistance from a baseline value, and $C(\Delta r)$ is the radius of curvature in mm. Values of these coefficients computed for one actuator are given in Table IV.

The radius of curvature C is then converted to a deflection angle of the tip for a given change in electrical resistance:

$$\theta(\Delta r) = \frac{L}{C(\Delta r)} \quad (3)$$

where $\theta(\Delta r)$ is the relationship between tip angle and resistance and L is the length of the sensor. This fit was done for five actuators, each one tested four separate times (Figure 9).
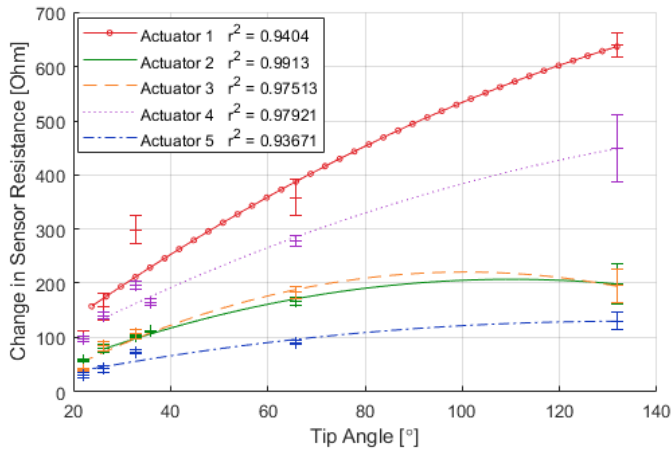
Fig. 9: Change in electrical resistance from a baseline during constant curvature tests on five actuators. Each actuator was bent to five different angles, with four samples per angle. A 2nd-order best fit curve to the data for each actuator is shown. Error bars show 95% (2σ) confidence bounds on measured resistance.
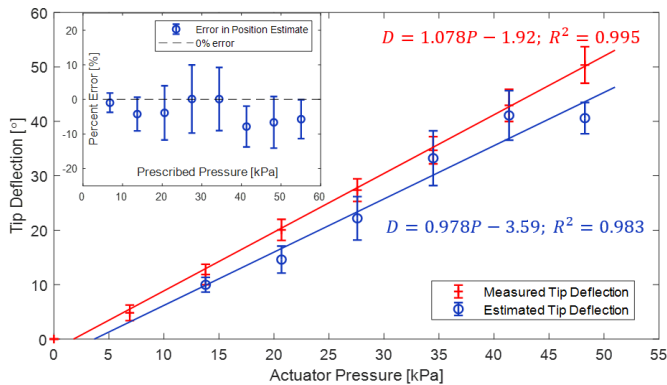

Fig. 10: Angle of the distal end of the actuator D at prescribed internal pressures P as measured using image processing (-) and as estimated by an actuator (O). Position estimate data is shown for a single calibrated sample (actuator 4 in Figure 9) . Error bars show 95% (2σ) confidence bounds. The inset plot shows % error in estimated position across $50°$ of actuation. For example, at 48 kPa the actuator estimates its position with $-6\pm7\%$ error, with 95% confidence. Data were collected at 40 Hz.

The baseline electrical resistance, as well as the slope of the response curve, is unique to each actuator and, as such, each actuator will have a unique calibration.

TABLE IV: Best-Fit Coefficients Example, $C(\Delta r)$

a_0	1.174e-3 mm/Ω^2	a_1	-1.085 mm/Ω	a_2	2.776e2 mm

The actuator's unique calibration then allows an estimation of the tip's deflection as the actuator is pressurized (Figure 10). We validated the model by subjecting the actuator to an increasing set of step pressures, measuring the deflection (Figure 5), reading the associated resistance and converting it to deflection using the calibrated model. This calculated deflection was then compared to the measured deflection (Figure 10). The comparison shows that the self-sensing actuator estimates its position to within $\pm10\%$ over bend angles up to $50°$ with 95% confidence.

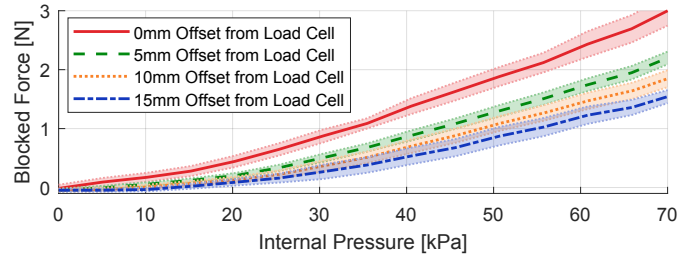This design is capable of bending $100°$ with 100 kPa and

Fig. 11: Force generated at the tip of the actuator for various applied pressures within the test fixture's digital range. Each curve was collected with a different distance between the undeflected actuator and the load cell and consists of 4 actuation cycles for each of the 5 actuators. Data were collected at 40 Hz. Shaded regions show 95% (2σ) confidence bounds on measured force.

no load (Figure 5) and generating a force at the tip of the actuator of 3 N at 70 kPa (Figure 11). The characterization of the force was done at four different deflections to understand the potential grasping force that the actuators could impart on various sized objects (Figure 11). The data were collected for five actuators under four actuation cycles.

VI. FUTURE WORK

This method for manufacturing self-sensing, soft actuators implies several avenues for future investigation. Potential strain gauge improvements include exploring other materials as well as optimizing the geometry of the gauge, which could improve the sensitivity and durability of the sensor. The availability of conductive filaments is currently limited, but commercially available conductive HIPS (BlackMagic3D) does exist, which could be compared against the doped PLA used here. Several low-cost filament-puller systems are now available, which could allow the investigation of custom filaments, with potentially higher strain gauge-factors.

In addition to exploring sensor improvements, optimizing the geometry of the actuator to minimize out of plane deformation is an avenue to be explored. Such exploration would help to reduce disturbances while the actuator is being utilized in a robotic end effector. In contrast to approaches that manually-integrate strain sensors, our approach enables potentially large numbers of strain sensors to be incorporated within a single actuator, enabling more granular measurements of the actuator's state. We have shown that these sensors can be used to detect contact (Figure 8 lower); numerous small sensors distributed throughout the design could enable force and touch sensing, while maintaining the compliant, low-cost, and durable qualities that make soft robotics appealing. Finally, future work could include integration of the self-sensing actuator into larger robotic systems; Figure 1 provides an example. This includes developing control laws suited to compliant actuators, or integrating it with printed pumps [28].

VII. CONCLUSION

To summarize this work: a novel, multi-material, self-sensing, soft actuator has been presented which is automatically fabricated with no human interaction and requires no post processing. The sensor-actuators are easily reproducible, requiring only two materials, each of which are compatible

with inexpensive, commercially available FFF printers. By leveraging the geometric complexity and ability to fabricate with multiple materials that additive manufacturing offers, we have created a self-sensing soft actuator that simultaneously offers high force and compliance. We have contributed an easily reproducible, *truly* print-in-place, soft, self-sensing robotic actuator.

VIII. Bibliography

References

[1] B. Mosadegh et al. "Pneumatic networks for soft robotics that actuate rapidly". In: *Advanced Functional Materials* 24.15 (2014), pp. 2163–2170.

[2] A. Zolfagharian et al. "Evolution of 3D printed soft actuators". In: *Sensors and Actuators, A: Physical* 250 (2016), pp. 258–272.

[3] R. Pelrine et al. "High-field deformation of elastomeric dielectrics for actuators". In: *Materials Science and Engineering C* 11.2 (2000), pp. 89–100.

[4] E. Acome et al. "Hydraulically amplified self-healing electrostatic actuators with muscle-like performance". In: *Science* 359.6371 (2018), pp. 61–65.

[5] M. T. Tolley et al. "An untethered jumping soft robot". In: *IEEE International Conference on Intelligent Robots and Systems* Iros (2014), pp. 561–566.

[6] R. F. Shepherd et al. "Using explosions to power a soft robot". In: *Angewandte Chemie - International Edition* 52.10 (2013), pp. 2892–2896.

[7] Filip Ilievski et al. "Titelbild: Soft Robotics for Chemists (Angew. Chem. 8/2011)". In: *Angewandte Chemie* 123.8 (2011), pp. 1765–1765.

[8] S. Joshi and J. Paik. "Multi-DoF Force Characterization of Soft Actuators". In: *IEEE Robotics and Automation Letters* 4.4 (2019), pp. 1–1.

[9] H. Lipson. "Challenges and Opportunities for Design, Simulation, and Fabrication of Soft Robots". In: *Soft Robotics* 1.1 (2014), pp. 21–27.

[10] H. Zhang et al. "Design and development of a soft gripper with topology optimization". In: *IEEE International Conference on Intelligent Robots and Systems* 2017-Septe (2017), pp. 6239–6244.

[11] H.K. Yap et al. "High-Force Soft Printable Pneumatics for Soft Robotic Applications". In: *Soft Robotics* 3.3 (2016), pp. 144–158.

[12] M. Schaffner et al. "3D printing of robotic soft actuators with programmable bioinspired architectures". In: *Nature Communications* 9.1 (2018).

[13] O. Byrne et al. "Additive manufacture of composite soft pneumatic actuators". In: *Soft Robotics* 5.6 (2018), pp. 726–736.

[14] O. D. Yirmibesoglu et al. "Direct 3D printing of silicone elastomer soft robots and their performance comparison with molded counterparts". In: *2018 IEEE International Conference on Soft Robotics, RoboSoft 2018* (2018), pp. 295–302.

[15] R. L. Truby et al. "Soft Somatosensitive Actuators via Embedded 3D Printing". In: *Advanced Materials* 1706383 (2018), pp. 1–8.

[16] B. Shih et al. "Design considerations for 3D printed, soft, multimaterial resistive sensors for soft robotics". In: *Frontiers Robotics AI* 6.APR (2019), pp. 1–12.

[17] R. Mutlu et al. "3D Printed Flexure Hinges for Soft Monolithic Prosthetic Fingers". In: *Soft Robotics* 3.3 (2016), pp. 120–133.

[18] R. MacCurdy et al. "Printable Hydraulics: A Method for Fabricating Robots by 3D Co-Printing Solids and Liquids". In: *IEEE International Conference on Robotics and Automation (ICRA)*. 2016, pp. 3878–3885.

[19] D. K. Patel et al. "Highly Stretchable and UV Curable Elastomers for Digital Light Processing Based 3D Printing". In: *Advanced Materials* 29.15 (2017), pp. 1–7.

[20] B. N. Peele et al. "3D printing antagonistic systems of artificial muscle using projection stereolithography". In: *Bioinspiration and Biomimetics* 10.5 (2015), p. 55003.

[21] C. A Manion, M. Fuge, and S. Bergbrieter. "Modeling and Evaluation of Additive Manufactured HASEL Actuators *". In: *International Conference on Intelligent Robots and Systems (IEEE/RSJ)*. 2018.

[22] M. A. H. Khondoker, N. Baheri, and D. Sameoto. "Tendon-Driven Functionally Gradient Soft Robotic Gripper 3D Printed with Intermixed Extrudate of Hard and Soft Thermoplastics". In: *3D Printing and Additive Manufacturing* 6.4 (2019), pp. 191–203.

[23] S. Mousavi et al. "An Ultrasensitive 3D Printed Tactile Sensor for Soft Robotics". In: *arXiv preprint* (2018).

[24] B. Shih et al. "3D printed resistive soft sensors". In: *2018 IEEE International Conference on Soft Robotics, RoboSoft 2018* (2018), pp. 152–157.

[25] F. Spina et al. "Directly 3D-printed monolithic soft robotic gripper with liquid metal microchannels for tactile sensing". In: *Flexible and Printed Electronics* (2019), p. 035001.

[26] C. Tawk et al. "Design , Modeling and Control of a 3D Printed Monolithic Soft Robotic Finger with Pneumatic Self-Sensing Chambers". In: *IEEE Transactions on Robotics*. 2019.

[27] ASTM D1876-08. "Standard Test Method for Peel Resistance of Adhesives (T-Peel Test)". In: *ASTM Book of Standards* 15.06.May (2015), pp. 5–7.

[28] V. Cacucciolo et al. "Stretchable pumps for soft machines". In: *Nature* 572.7770 (2019), pp. 516–519.

[29] L. Ding et al. "Design of soft multi-material pneumatic actuators based on principal strain field". In: *Materials and Design* 182 (2019), p. 108000.

[30] J. Fras et al. "Soft fluidic rotary actuator with improved actuation properties". In: *IEEE International Conference on Intelligent Robots and Systems* 2017-Septe (2017), pp. 5610–5615.